CRISPR/Cas-assisted Nanoneedle Sensor for ATP Detection in Living Cells

Hongki Kim[1,2], Chenlei Gu[1,3], Salman Ahmad Mustfa[1,†], Davide Alessandro Martella[1], and Ciro Chiappini[1,3]*

1 Centre for Craniofacial and Regenerative Biology, King's College London, London, SE1 9RT, UK

2 Department of Chemistry, Kongju National University, Gongju 32588, Republic of Korea

3 London Centre for Nanotechnology, King's College London, London, SE1 9RT, UK

† current address: AstraZeneca, Granta Park, Great Abington, Cambridge, CB21 6GH, United Kingdom

*correspondence to Dr. Ciro Chiappini: ciro.chiappini@kcl.ac.uk

Abstract
The clustered regularly interspaced short palindromic repeats (CRISPR)-associated protein (Cas) (CRISPR/Cas) systems have recently emerged as a powerful molecular biosensing tool based on their collateral cleavage activity due to their simplicity, sensitivity, specificity, and broad applicability. However, the direct application of collateral cleavage activity for in-situ intracellular detection is still challenging. Here, we debut a CRISPR/Cas-assisted nanoneedle sensor (nanoCRISPR) for intracellular adenosine triphosphate (ATP), which avoids the challenges associated with intracellular collateral cleavage by introducing a two-step process of intracellular target recognition followed by extracellular transduction and detection. ATP recognition occurs by first presenting in the cell cytosol an aptamer-locked Cas12a activator conjugated to nanoneedles; the recognition event unlocks the activator immobilized on the nanoneedles. The nanoneedles are then removed from the cells and exposed to the Cas12a/crRNA complex, where the activator triggers the cleavage of a ssDNA fluorophore-quencher pair, generating a detectable fluorescence signal. NanoCRISPR has an ATP detection limit of 246 nM and a dynamic range from 1.56 μM to 50 μM. Importantly, nanoCRISPR can detect intracellular ATP in 30 min in live cells without impacting cell viability. We anticipate that the nanoCRISPR approach will contribute to broaden the biomedical applications of CRISPR/Cas sensors for the detection of diverse intracellular molecules in living systems.

Introduction

Recently, the clustered regularly interspaced short palindromic repeats (CRISPR)-associated nuclease (Cas) (CRISPR/Cas) system, originally identified in bacteria and archaea, has gained considerable attention in molecular diagnostics due to its superb specificity of molecular target recognition, fast turnaround time, convenient isothermal reaction, and signal amplification capabilities.[1–3] Several CRISPR-based sensing approaches such as DETECTR (DNA endonuclease-targeted CRISPR trans reporter), SHERLOCK (specific high-sensitivity enzymatic reporter unlocking), HOLMES (one-hour low-cost multipurpose highly efficient system), and others, have been developed with high sensitivity and specificity.[4–9] For example, DETECTR showed attomolar sensitivity, HOLMES achieved a limit of detection (LOD) around 10 aM, and SHERLOCKv2 enabled the multiplexed sensing of target detection at zeptomolar sensitivity.[4–6] Among diverse Cas proteins, Cas12a (a class of type V nuclease) shows a unique collateral cleavage activity that can non-specifically cleave single-stranded DNA substrates (termed as *trans*-cleavage) upon recognition of the correct target DNA by crRNA.[4,6] By adopting single-stranded DNA labeled with a fluorophore and quencher pair, the collateral cleavage activity can generate enormously amplified signals in response to a target analyte, including not only nucleic acid but also protein, transcription factors, and small molecules.[10–12] In particular, Cas12a-based sensors can rapidly and sensitively detect ATP levels.[13–17] Yet Cas12a collateral cleavage is not suited to in-situ intracellular detection as it requires the co-delivery of multiple components (the Cas12a RNP, the crRNA, and the DNA substrates) and risks indiscriminate off-target cleavage of nucleic acids essential to cell function.[18,19] Such limitation prevents the use of this sensitive and specific sensing approach to monitor live cells.

Nanomaterial-based approaches are well suited to enable intracellular sensing.[3] Numerous strategies involving nanoparticles, nanorods, and nanowires have been extensively explored.[20,21] In particular, nanoneedles, vertically-aligned arrays of high aspect ratio nanostructures,[22] have been widely used to access the intracellular space with minimal disruption of cell functions and sense intracellular biomolecules.[23–28] Porous silicon nanoneedles have a high surface area to volume ratio which provides abundant binding sites for target capture/interaction, with the potential to enhance sensing performance.[24–27] They are bioresorbable, making them suitable for *in vivo* diagnostics with minimal concerns for patient health. Porous silicon nanoneedles can successfully detect the intracellular activity of tumor biomarker enzymes in living cells and clinical samples using fluorescent-based approaches. While enzymatic biomarkers can be detected intracellularly, relying on their intrinsic signal amplification capacity, detecting non-enzymatic biomarkers is more challenging. Nonetheless, nanoneedles decorated with suitable capture probes can effectively "fish" target biomolecules from living cells, and do so repeatedly for longitudinal analysis of cell state.[29–32] Fished molecules can be detected using ex-situ amplification strategies.[33] Such capability provides a unique avenue to combine the specificity and sensitivity of Cas12a-based sensing with unprecedented access to the intracellular space provided by nanoneedles for the detection of non-enzymatic intracellular targets.

In particular, adenosine triphosphate (ATP) is the primary energy carrier molecule for living organisms, playing a vital role in biochemical reactions and cellular metabolic processes.[34] The intracellular levels of ATP are tightly regulated to insure cell health and direct key biological processes, including cell division, self-renewal, and differentiation.[35,36] ATP assays are a cornerstone of molecular biology for monitoring cell viability, proliferation, and cytotoxic events, yet to date ATP quantification is a destructive process requiring cell lysis. Monitoring ATP dysregulation can provide diagnostic information for cardiovascular, neurodegenerative, and mitochondrial diseases, hypoxia, hypoglycemia, ischemia, and the

progression, invasiveness, and drug resistance of malignant tumors.[36–43] Therefore, accurate detection and quantification of ATP are highly important to understand biological systems and improve diagnosis and treatment. Luciferase-based approaches for ATP detection are a workhorse in molecular biology, with good sensitivity for quantification from cell lysates.[44] Other methods for ATP analysis include electrophoresis, isotope tracing, high-performance liquid chromatography and so on.[45–47] Although these methods have been proved to be effective for ATP detection *in vitro*, they are time-consuming, require tedious sample preparations, and cannot be used in living cell. FRET-based approaches can monitor ATP levels with single cell resolution in live system but use genetically-encoded reporters which require complex genetic engineering and cannot be deployed in a diagnostic setting.[48]

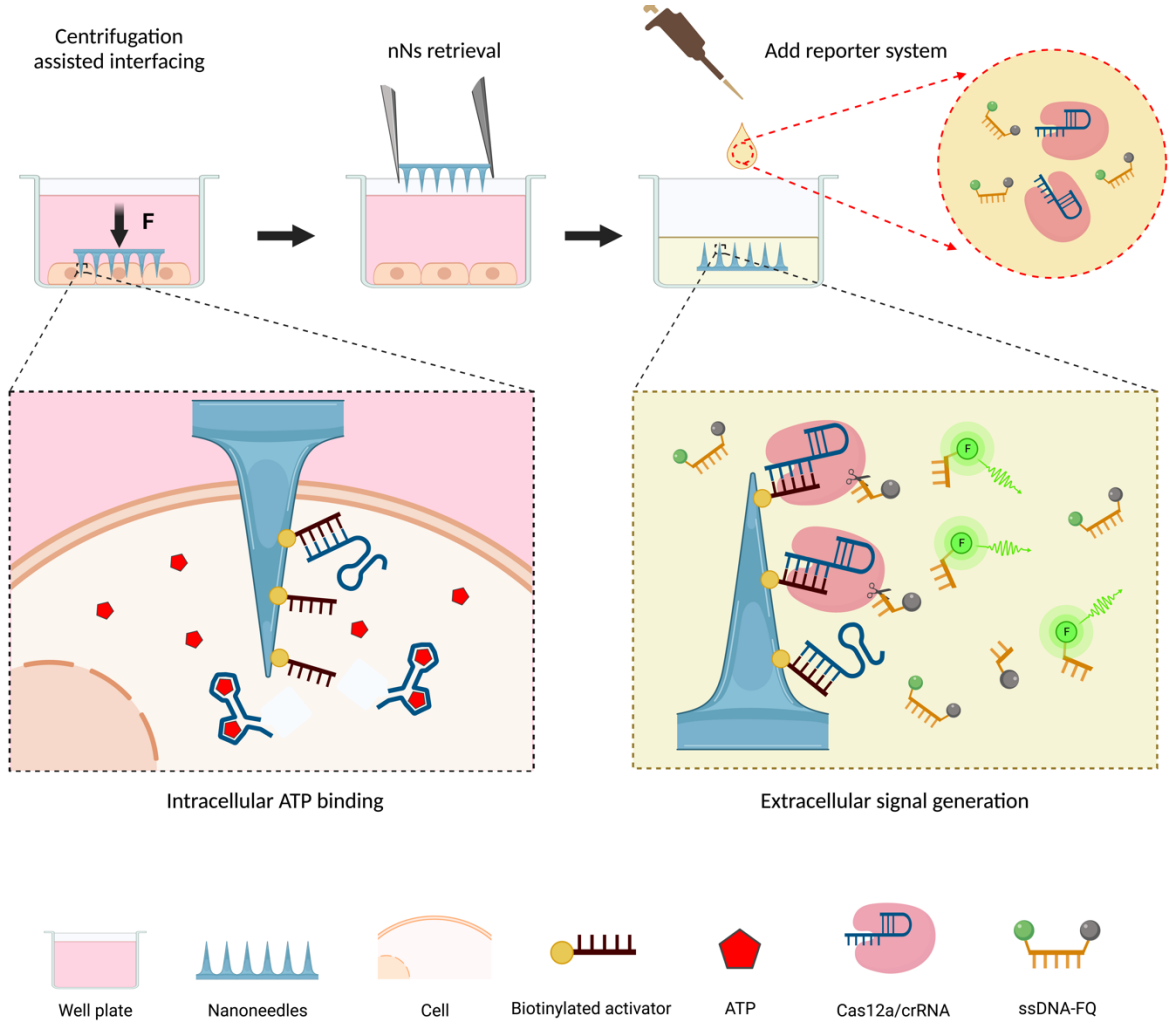

Figure 1. Schematic representation of the CRISPR/Cas-assisted nanoneedle sensor for intracellular detection of ATP. *The locked activator-modified nanoneedles are placed in the cell culture well with the nanoneedles facing toward cells (nanoneedles on top interfacing), and the whole setup is centrifuged. The centrifugation interfaces the nanoneedles with the cells, presenting the aptamers in the cytosol where they bind to intracellular ATP. When bound to ATP, the aptamer is released and unlocks the activator. After centrifugation, the nanoneedles are retrieved and incubated with the reporter system containing a Cas12a/crRNA*

complex and a ssDNA F-Q. The exposed activator triggers the cleavage of ssDNA-FQ by Cas12a/crRNA, yielding a detectable fluorescent signal.

In this study, we detect intracellular ATP levels in a live cell culture using a nanoneedle-based approach which relies on Cas12a amplification. We functionalize the surface of porous silicon nanoneedles with a Cas12 activator locked by an ATP aptamer. The nanoneedles are interfaced with cells displaying the sensing element in the cytosol; upon intracellular ATP recognition the aptamer configurational changes release the activator. The retrieved nanoneedles are incubated with the Cas12 detection system which provides an assessment of the intracellular ATP levels in the cell culture.

Results

NanoCRISPR: The CRISPR/Cas-assisted nanoneedle sensor

NanoCRISPR is a CRISPR/Cas-assisted nanoneedle sensor for ATP detection, which operates in two steps. It first exploits the intracellular access provided by nanoneedles to expose an aptamer-locked CRISPR/Cas12 activator to cytosolic ATP, and then generates an amplified signal by exposing the unlocked activator to CRISPR/Cas12 outside the cell (Figure 1). The sensor was assembled using conical porous silicon nanoneedles with 2.4 μm length, 150 nm tip diameter, 2 μm spacing and 40 % porosity. The surface of nanoneedles was oxidized by O_2 plasma and then functionalized with 3-aminopropyltriethoxisilane (APTES) (Figure S1).
Biotin was conjugated to the amine-functionalized nanoneedles followed by the addition of polystreptavidin . The locked activator composed of an ATP aptamer strand locking the biotin-labeled activator strand was immobilized onto nanoneedles through interaction with the polystreptavidin. For intracellular ATP detection, the nanoneedles functionalized with the locked activator were centrifuged over adherent cells in culture with the needles facing toward cells. Assisted interfacing by centrifugation can increase membrane permeability, promoting access to the cell without additional perturbation.[28,49] Following centrifugation, the nanoneedles were retrieved and exposed to a preassembled Cas12a/crRNA complex alongside single-stranded DNA labeled with a fluorophore (FAM) and a quencher (IABkFQ) (named ssDNA-FQ). During cell interfacing, the aptamer binds to the ATP present in the cell, undergoing a conformational change which leads to its release and exposes the activator. The exposed activator remains on the nanoneedles and is specifically recognized when exposed to Cas12a/crRNA, thereby activating the cleavage of ssDNA-FQ, yielding a fluorescent signal correlated to the amount of intracellular ATP, which is measured in a plate reader. With this approach, the synergistic combination of the non-perturbing intracellular access granted by nanoneedle array and the amplifying capacity of the CRISPR system could allow for simple and rapid detection of trace ATP in living cells.

nanoCRISPR assembly

To determine the feasibility of our approach, we first verified the activation of the Cas12a by target ATP by agarose gel electrophoresis analysis using a 50 nt ssDNA as the substrate (Figure 2a). The ssDNA (lane 1) was cleaved by the activated Cas12a in the presence of the activator (lane 2) but not in the absence of activator (lane 5), indicating that the activator is responsible for triggering the ssDNA cleavage of Cas12a/crRNA. In the presence of ATP and a locked activator (lane 3), we observed ssDNA digestion similar to the unlocked activator (lane 2), indicating that target ATP binding event effectively unlocked the activator and thus activated the cleavage effect on ssDNA. On the other hand, in absence of ATP the activator remained locked by the aptamer, as no cleavage (lane 4) was observed.

We then validated that the system retained its functionality when assembled on nanoneedles (Figure 2b). When the activator strands were immobilised on nanoneedles, a

remarkable fluorescence signal was obtained after incubation with ssDNA-FQ and Cas12a/crRNA (violet spectrum in Figure 2b). Instead, a negligible signal was observed when

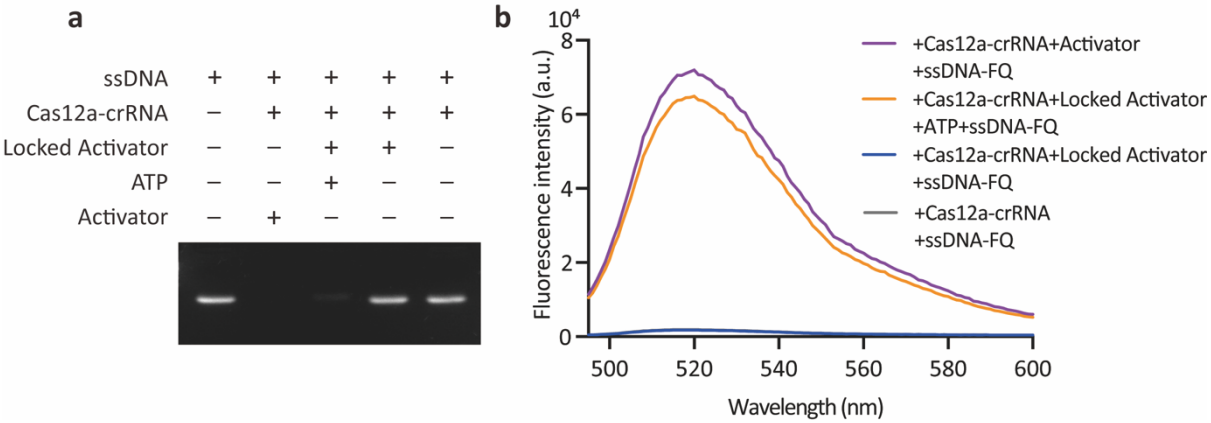

Figure 2. Validation of the nanoCRISPR sensor for ATP detection. *a) Agarose gel electrophoresis analysis of CRISPR/Cas12 activation upon ATP detection by the locked activator in solution. ssDNA without secondary structure was used as the substrate (Lane 1: ssDNA, Lane 2: ssDNA + Cas12a/crRNA + Activator, Lane 3: ssDNA + Cas12a/crRNA + Locked Activator + ATP, Lane 4: ssDNA + Cas12a/crRNA + Locked Activator, and Lane 5: ssDNA + Cas12a/crRNA). b) Fluorescent signal generation from the assembled nanoCRISPR sensor upon ATP detection. (purple spectrum: Activator immobilised on nanoneedles + Cas12a/crRNA + ssDNA F-Q, gray spectrum: bare nanoneedles + Cas12a/crRNA + ssDNA F-Q, orange spectrum: Locked Activator immobilised on nanoneedles + ATP + Cas12a/crRNA + ssDNA F-Q, and blue spectrum: Locked Activator immobilised on nanoneedles + Cas12a/crRNA + ssDNA F-Q).*

incubating ssDNA-FQ and Cas12a/crRNA with nanoneedles in the absence of the activator (gray spectrum in Figure 2b). We then tested the locked activator immobilized on nanoneedles. We used the optimal molar ratio of 2 ATP aptamers per each activator; this ratio yields minimal non-specific unlocking of the activator as shown by the low background fluorescence when incubated with the Cas12a/crRNA+ ssDNA-FQ in the absence of ATP (Figure S2).[13,17] When this system was incubated with 200 µM ATP and Cas12a/crRNA with ssDNA-FQ, a strong fluorescence signal was observed (orange spectrum, Figure 2b). In contrast, when ATP was absent, a weak fluorescence signal was measured (dark blue spectrum, Figure 2b). Taken together, these results indicate that the sensor assembled on the nanoneedles can detect target ATP by activating the ssDNA cleavage activity of Cas12a, corroborating the results from agarose gel electrophoresis analysis.

Sensitivity and Selectivity of nanoCRISPR

To examine the analytical performance of the proposed nanoCRISPR sensor, we measured the fluorescence spectra in the presence of ATP concentrations ranging from 0 to 200 µM. By evaluating the fluorescence intensity as a function of reaction times, we determined an optimal incubation of 20 min (Figure S3). Fluorescence signal gradually decreased with decreasing concentrations of ATP (Figure 3). Furthermore, the signal was still visible even at the lowest assessed concentration of 0.78 µM, compared with the signal of a blank sample (Figure 3a). The fluorescence intensity measured at 520 nm linearly increased with ATP concentration in the range from 1.56 µM to 50 µM, with a linear fit $y = 1246x + 1587$ (Figure 3b). The R^2 value of 0.97 indicates a robust linear relationship between fluorescence signal and ATP concentration. Using the limit of detection (LOD) formula $LOD = 3 \cdot sb/m$, where sb is the standard deviation of fluorescence response for blank samples and m is the

slope of the calibration curve, the LOD of nanoCRISPR for target ATP was estimated to be 246 nM. This LOD is approximately 5-fold lower than that of commercial ATP kits and comparable to that of other CRISPR-based sensing systems reported previously.[13–16]

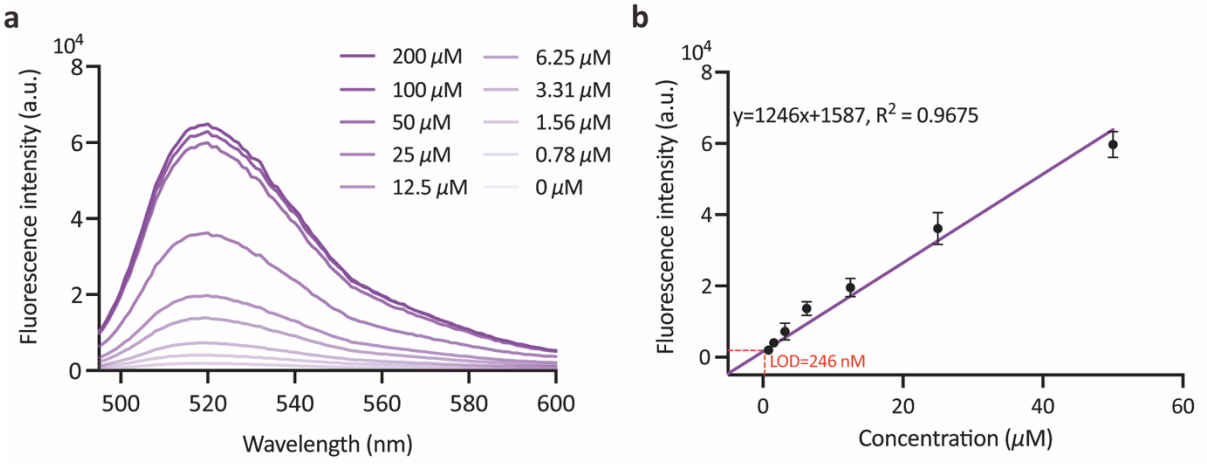

Figure 3. Performance of the nanoCRISPR sensor for the detection of ATP*. a) Fluorescence response of the nanoCRISPR in the presence of ATP ranging from 0 µM to 200 µM (0, 0.78, 1.56, 3.13, 6.25, 12.5, 25, 50, 100, 200 µM) b) Linear regression of the fluorescence intensity at 520 nm as a function of ATP concentration. Data represent the average ± standard deviation from five measurements.*

The selectivity of nanoCRISPR was investigated by comparing the fluorescence response for ATP with that for the competing nucleotide-triphosphate analogs UTP, CTP, and GTP (Figure 4a) at 200 µM concentration. Fluorescence intensity at 520 nm for ATP was more than 14 times stronger compared to the analogs (Figure 4b). These results indicate that nanoCRISPR is sensitive and highly specific for ATP.

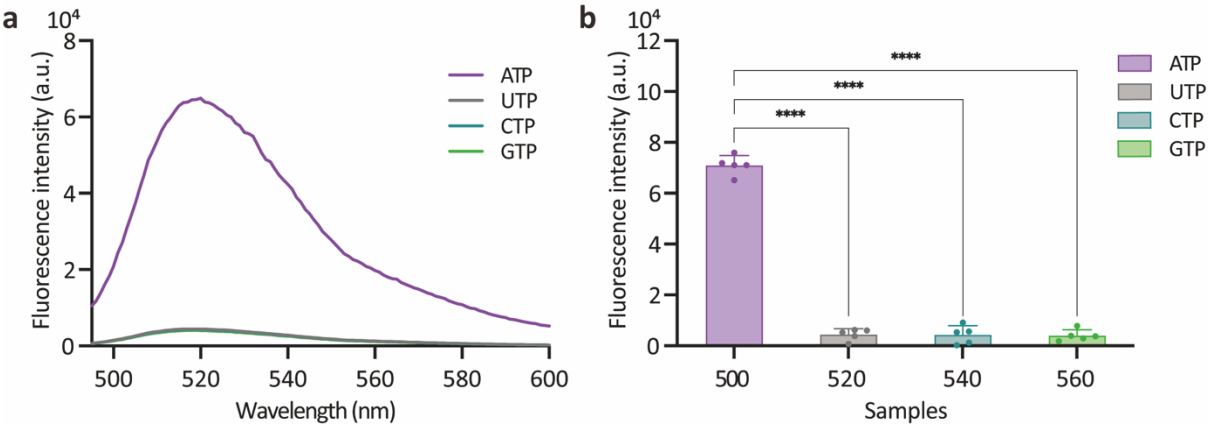

Figure 4. Selectivity of nanoCRISPR for ATP detection. *a) Fluorescence spectra measured from nanoCRISPR after exposure to 200µm of ATP, UTP, CTP, and GTP. b) Corresponding histograms for the fluorescence intensity at 520 nm as measured from the fluorescence spectra. Data represent mean plus standard deviation from five measurements. One way ANOVA with Tukey post-test; ****p<0.0001.*

Intracellular detection of ATP

To demonstrate the feasibility of our proposed nanoCRISPR approach for intracellular ATP sensing, we prepared cultures with 30,000 and 50,000 HEK-293 cells, and cells treated with oligomycin, which is a known inhibitor of mitochondrial ATP synthase. We evaluated the intracellular ATP detection performance based on the modality of interfacing, by comparing cells cultured on nanoneedles (nanoneedles on bottom, nN-B) with nanoneedles placed over cells in culture (nanoneedles on top, nN-T) (Figure 5). All modalities of interfacing were assisted by centrifugation. For nN-B interfacing, a distinct fluorescence signal was obtained from all samples, compared to that of dead cells (Figure 5a). However, the fluorescence intensities obtained from HEK-293 and oligomycin-treated HEK-293 cells were quite similar at a centrifugation speed of 300 rpm. A clear difference in fluorescence intensities between HEK-293 and oligomycin-treated HEK-293 was observed only when a centrifugation speed of 600 rpm was applied. Furthermore, the nN-B interfacing showed limited ability to discriminate between 30,000 and 50,000 cells in culture, regardless of centrifugation speed. On the other hand, for nN-T interfacing the difference between the fluorescence signal of untreated and oligomycin-treated cell was clearly seen at both 300 rpm and 600 rpm (Figure 5b). The average relative signal difference between treated and untreated cells was ~57%, which is ~1.7 times larger than the signal difference measured for nN-B interfacing. Similarly, nN-T interfacing could discriminate between 30,000 and 50,000 cells at both centrifugation speeds. These results show that the nanoCRISPR sensor can detect intracellular ATP concentration, and has better sensitivity when using nN-T interfacing.

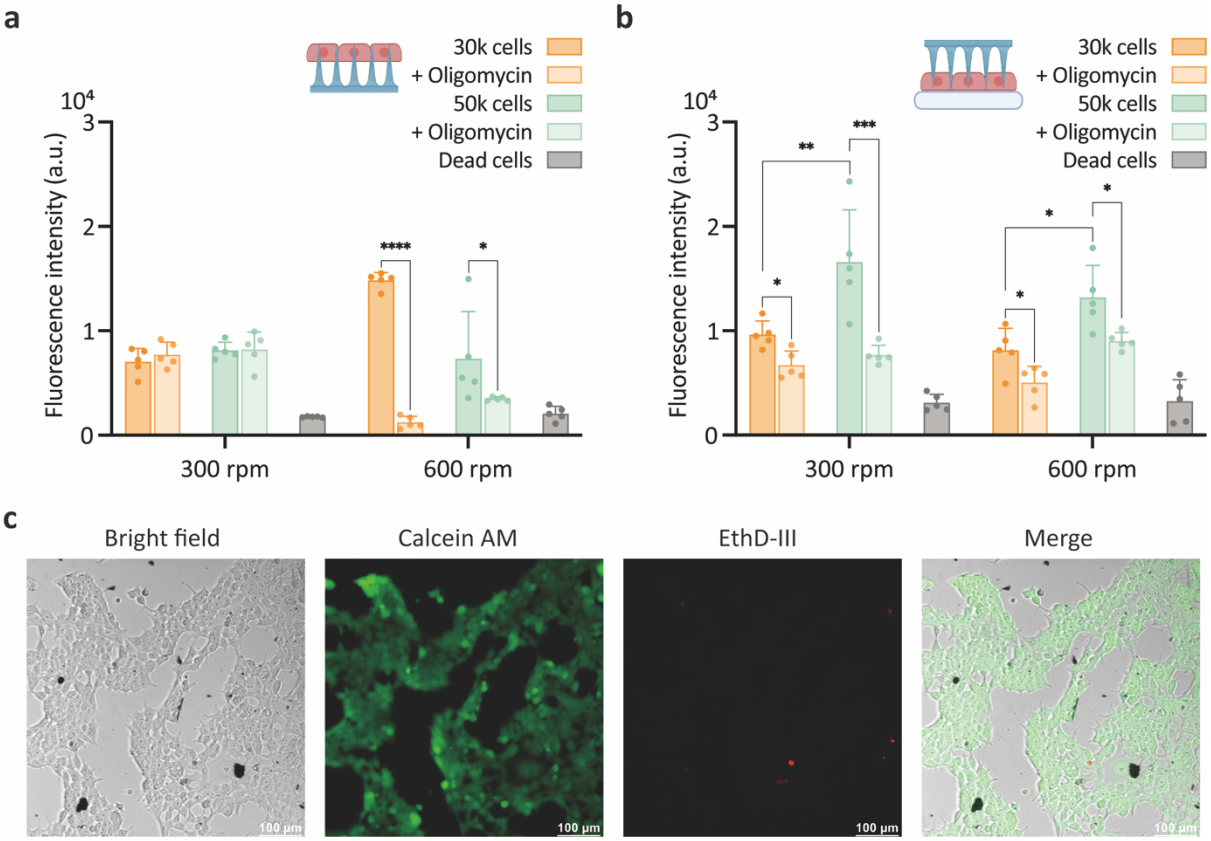

Figure 5. Intracellular detection of ATP using nanoCRISPR in live cells. *a) Comparison of the fluorescence signal detected at 520 nm for nanoCRISPR interfaced nanoneedles on bottom. Individual groups include HEK-293 cells at 30k and 50k cell concentration, with and without oligomycin treatment and dead cells, at the two centrifugation speeds of 300 rpm and 600 rpm. b) Comparison of the fluorescence signal detected at 520 nm for nanoCRISPR interfaced nanoneedles on top. Individual groups include HEK-293 cells at 30k and 50k cell concentration,*

*with and without oligomycin treatment and dead cells, at the two centrifugation speeds of 300 rpm and 600 rpm. Data represent mean plus standard deviation from 5 measurements. Statistical analysis was performed by two-way ANOVA with Holm-Sidak multiple-comparison test. * p<0.0332, ** p<0.021, *** p<0.0002, ****p<0.0001 c) LIVE/DEAD assay on 50k HEK-293 cells following nN-T interfacing with nanoCRISPR at 300RPMs. Left to right: bright field; green fluorescence from Calcein AM indicating live cells; red fluorescence from EthD-I indicating dead cells; merged channels. Scale bar is 100 µm.*

The ATP concentration in a single cell was calculated by considering the linear fit of fluorescence intensity as a function of ATP concentration calculated in Figure 3b and the volume and number of cells

$$[ATP]_{cell} = \frac{F - 1587}{1246} \cdot \frac{V_{sol}}{N \cdot V_{cell}}$$

Where $[ATP]_{cell}$ represents ATP cell concentration, F is the fluorescent signal at 520 nm, V_{sol} is the volume of the sensing solution, V_{cell} is the volume of an individual cell and N is the number of cells interfaced. For nN-T interfacing, $[ATP]_{cell}$ measured in untreated HEK-293 cells was 1.138±0.26 mM. This result is in agreement with previous reports indicating cellular ATP concentrations ranging from 1 to 10 mM.[50]

We determined the impact of nanoneedle interfacing on cells by live/dead assay to assess the cell viability (Figure 5c). For nN-T interfacing, regardless of centrifugation speed, we could not detect evidence of dead cells, indicating that nanoCRISPR enables intracellular ATP detection without major cell perturbation.

Conclusion

We developed nanoCRISPR as an intracellular ATP sensing platform combining nanoneedle technology for intracellular access with aptamer ATP recognition and CRISPR/Cas12a amplification. We assembled on nanoneedles a locked-activator sensor capable of selectively recognizing ATP, resulting in unlocking of the Cas12a activator, and triggering the cleavage of ssDNA-FQ by Cas12a, yielding a detectable fluorescent signal. NanoCRISPR can quantitatively detect ATP with a LOD of 246 nM and high selectivity against other triphosphate nucleotides. Moreover, by nanoneedle on top interfacing with the assistance of centrifugation, nanoCRISPR can detect intracellular ATP in living cells in 30 minutes. The sensor can discriminate between different intracellular ATP concentration and different cell numbers without impacting cell viability. This approach opens the way to noninvasive longitudinal monitoring of cell viability for long-term culture and to monitor the effects of challenges to cells. It is anticipated that the simple, rapid, and sensitive nanoCRISPR sensor can be applied in biomedical studies and cancer research for monitoring dynamic ATP levels and extended for detecting a range of other analytes in living sample.

Experimental Section

Materials. The all DNA and RNA sequences synthesized and purified with HPLC by Integrated DNA Technologies (UK) are listed in Table S1. Cas12a and related all buffer were purchased from Integrated DNA Technologies. Adenosine 5′-triphosphate (ATP), cytidine 5′-triphosphate (CTP), guanosine 5′-triphosphate (GTP), uridine 5′-triphosphate (UTP), and RNase inhibitor were purchased from NEW ENGLAND BioLabs Inc. (Ipswich, UK). NHS-Biotin was purchased from Sigma-Aldrich, Inc (H1759-100 MG). Polystreptavidin R buffer was purchased from BioTeZ Berlin-Buch GmbH. 4-(2-hydroxyethyl)-1-piperazineethanesulfonic acid (HEPES), with 3-aminopropyltriethoxisilane (APTES), and other chemicals were purchased from Sigma-Aldrich, Inc.

Fabrication of porous silicon nanoneedles. Porous silicon nanoneedles were fabricated according to established protocols .[24] First, a 160 nm layer of silicon-rich silicon nitride was deposited by chemical vapour deposition onto p-type, 100 mm, <100> silicon wafers. Second, the substrate was patterned with a square array of dots having diameter of 600 nm and pitch of 2 μm, by UV photolithography. NR9-250P photoresist (Futurrex Inc, USA) was spin coated on the substrate to form a 220 nm thick layer, by using the following steps 500 RPM / 1000 RPMS / 5 s, 4000 RPM / 5000 RPMS / 40 s. Prebaking of the substrate was performed on a hotplate at 70 °C for 180 s, then the substrate was placed in contact with the mask by hard vacuum contact by using a MA6 mask aligner (K. Suss GMBH, Germany) and exposed to UV. After exposure, post-baking of the substrate was performed on a hotplate at 100 °C for 60 s. The photoresist was developed in a dilution of the developer 3:1 RD6:H_2O, for 12 s (Futurrex Inc, USA), then rinsed with excess water and dried with stream of N_2. After photolithography, the pattern was transferred to the silicon nitride layer by reactive ion etching (RIE, NGP80 Oxford Instruments, UK) at 50 sccm CHF_3, 5 sccm O_2, 150 W forward power, 55 mTorr pressure, for 150 s. The remaining photoresist was stripped by acetone, the substrate was rinsed with isopropanol and dried with stream of N_2. The nitride pattern was then used to mask the silicon during metal assisted chemical etching (MACE), to form an ordered array of porous silicon pillars. Before MACE, the native oxide layer was removed by substrate dip in 10 % HF (Honeywell, USA) for 2 minutes. This was immediately followed by electroless Ag deposition in 100 ml of 20 mM $AgNO_3$ (Sigma Aldrich), 10% HF for 2 minutes. The substrate was rinsed with water, then isopropanol and dried with stream of N_2. The substrate undergoes MACE in 400 ml of a solution of 30 vol H_2O_2 (Sigma Aldrich) : 10% HF in volume ratio 1:99, for 3 min. To stop the etch, the wafer was dipped in H_2O, rinsed with excess H_2O and isopropanol, and dried with stream of N_2. The residual Ag is removed by dipping the substrate in gold etchant solution (Aldrich) for 10 min. The substrate is rinsed with excess H_2O, isopropanol and dried with stream of N_2. The conical structure of the nanoneedles was obtained by RIE (NGP80, Oxford Instruments, UK) at 20 sccm SF_6, 200 W forward power, 100 mTorr pressure, for 90 s. After the fabrication of the nanoneedles, the 100 mm wafer was diced in 4x4 mm square chips by using a dicing saw (Disco, DAD3220).

Surface functionalization of nanoneedles. The fabricated nanoneedles were oxidized by O_2 plasma for 10 min in the Low-pressure Plasma System (ZEPTO-W6, Diener electronic GmbH & Co). The oxidized surfaces of nanoneedle were functionalized with amine group by incubating with 2% APTES in ethanol for 3 hr. The nanoneedles were then washed 3 times with ethanol and dried for 1hr at 100 °C. Next, NHS-Biotin (100 μg/mL) was coated to the nanoneedles for 1 hr. After washing with PBS 5 times, the biotinylated nanoneeldes were reacted with poly-streptavidin (50 μg/mL) for 18 hr and washed with DI water 5 times. Finally, the biotinylated locked activator probes (5 μM) were added to the polystreptavidin/biotin/nanoneedles array. After washing with PBS 3 times, ATP aptamer-1 and aptamer-2 (10 μM) in a hybridization buffer solution(5X SSC, 750 mM NaCl and 75 mM trisodium citrate) were added to the locked activator functionalized nanoneeldes and incubated for 6 hr, followed by washing twice with the rinsing buffer solution (2X SSC and 0.05% wt Tween-20)

Preparation of Cas12a/crRNA complex and detection of ATP. The 10 μM crRNA (10 μL) was preincubated with 62 μM dCas9 (1.6 μL) in PBS buffer at RT for 30 min. After creating Cas12a/crRNA complex (1 μM), the complex was stored at 4 °C for up to 24 h before use. For the sensitivity analysis, 20 μL of reaction buffer (40 mM HEPES, 100 mM NaCl, 20 mM $MgCl_2$)

containing different concentrations of ATP was added onto the locked activator functionalized nanoneedle. After incubation of 5 min, 40 μL of 100 nM Cas12a/crRNA complex, 30 μL of 100 nM ssDNA F-Q, and 10 μL of reaction buffer were added and incubated for 20 min at 25 °C. After that, the enzymatic reaction was stopped by heating at 60 °C for 5 min and the fluorescence data was collected. For selectivity analysis, different nucleoside triphosphates were added into the locked activator functionalized nanoneedle and other procedures were the same as ATP sensitivity analysis.

Cell culture. HEK293-T cells were cultured in DMEM medium (Gibco) supplemented with 10% fetal bovine serum (FBS, Gibco), 1% penicillin-streptomycin (Gibco) and were incubated at 37°C with 5% CO_2. Mycoplasma contamination of the cells was tested to their standard levels of stringency. Cells were washed 3 times with DPBS (Sigma-Aldrich) and trypsinized. Cell were resuspended in DMEM and counted using hemocytometer before being seeded into the 96-well plate for the experiment. Oligomycin (Selleck Chemicals) was prepared 1 mg/mL as stock solution according to the manufacturer's protocol, and 2 μL was applied to the 200 μL cell culture system to make a final working concentration of 10 μg/mL for treatment.

Intracellular detection of ATP. For nanoneedles on top (nN-T) interfacing the nanoCRISPR device was placed to float on a culture medium with the nanoneedles facing toward cells, and then the whole setup was centrifuged at various speeds for 5 min. After centrifugation, more medium was immediately added to the culture well to remove the nanoneedle sensor by lifting above the cells. For nanoneedles on bottom interfacing (nN-B),the nanoneedles were placed at the bottom of a 96-well plate and 200 ul of medium containing the desired amount of cells was added. The whole setup was centrifuged at various speeds for 5 min. After removal, for either interfacing methodology, the nanoneedle was washed 3 times with PBS. Next, 100 nM Cas12a/crRNA complex, 100 nM ssDNA F-Q were added and incubated for 35 min at 25 °C. After that, the enzymatic reaction was stopped by heating at 60 °C for 5 min and the fluorescence data was collected.

Live/Dead assay. Calcein AM (BD Pharmingen™) 5 mM stock solution in DMSO was prepared and stored at -20°C according to the protocol. Live/dead staining mix was prepared by adding Calcein AM (1:2000) and Ethidium Homodimer III (EthD-III, Biotium) (1:1000) into Hank's Balanced Salt Solution (HBSS, Gibco). Cells in 96-well plate were HBSS washed once before adding the live/dead staining mix. After incubation at room temperature in the dark for 30 minutes, the cells were washed with HBSS once, then supplemented and left in HBSS for microscope imaging.

Instruments. Fluorescence data was collected in a CLARIOstar®Plus plate reader using 485 nm excitation and 520 nm emission. Gel imaging was carried out using U:Genius^3 system. Images were acquired by DMi8 inverted microscope with a 20X 0.8 NA dry objective.

Acknowledgements

CC Acknowledges funding from the European Research Council under the Starting Grant ENBION 759577. HK Acknowledges funding from National Research Foundation of Korea (NRF) grant funded by the Korea government (MSIT) (NRF-2022R1C1C1005761).

References

(1) Kaminski, M. M.; Abudayyeh, O. O.; Gootenberg, J. S.; Zhang, F.; Collins, J. J. CRISPR-Based Diagnostics. *Nat. Biomed. Eng.* **2021**, *5* (7), 643–656. https://doi.org/https://doi.org/10.1016/j.aca.2021.339180.

(2) Yue, H.; Huang, M.; Tian, T.; Xiong, E.; Zhou, X. Advances in Clustered, Regularly Interspaced Short Palindromic Repeats (CRISPR)-Based Diagnostic Assays Assisted by Micro/Nanotechnologies. *ACS Nano* **2021**, *15* (5), 7848–7859. https://doi.org/10.1021/acsnano.1c02372.
(3) Hu, T.; Chen, X. Nano for CRISPR. *ACS Nano* **2022**, *16* (6), 8505–8506. https://doi.org/https://doi.org/10.1021/acsnano.2c05431.
(4) Chen, J. S.; Ma, E.; Harrington, L. B.; Da Costa, M.; Tian, X.; Palefsky, J. M.; Doudna, J. A. CRISPR-Cas12a Target Binding Unleashes Indiscriminate Single-Stranded DNase Activity. *Science (80-.).* **2018**, *360* (6387), 436–439. https://doi.org/10.1126/science.aar6245.
(5) Gootenberg, J. S.; Abudayyeh, O. O.; Kellner, M. J.; Joung, J.; Collins, J. J.; Zhang, F. Multiplexed and Portable Nucleic Acid Detection Platform with Cas13, Cas12a and Csm6. *Science (80-.).* **2018**, *360* (6387), 439–444. https://doi.org/10.1126/science.aaq0179.
(6) Li, S. Y.; Cheng, Q. X.; Li, X. Y.; Zhang, Z. L.; Gao, S.; Cao, R. B.; Zhao, G. P.; Wang, J.; Wang, J. M. CRISPR-Cas12a-Assisted Nucleic Acid Detection. *Cell Discov.* **2018**, *4* (1), 18–21. https://doi.org/10.1038/s41421-018-0028-z.
(7) Gootenberg, J. S.; Abudayyeh, O. O.; Lee, J. W.; Essletzbichler, P.; Dy, A. J.; Joung, J.; Verdine, V.; Donghia, N.; Daringer, N. M.; Freije, C. A.; Myhrvold, C.; Bhattacharyya, R. P.; Livny, J.; Regev, A.; Koonin, E. V.; Hung, D. T.; Sabeti, P. C.; Collins, J. J.; Zhang, F. Nucleic Acid Detection with CRISPR-Cas13a/C2c2. *Science (80-.).* **2017**, *356* (6336), 438–442. https://doi.org/10.1126/science.aam9321.
(8) Harrington, L. B.; Burstein, D.; Chen, J. S.; Paez-Espino, D.; Ma, E.; Witte, I. P.; Cofsky, J. C.; Kyrpides, N. C.; Banfield, J. F.; Doudna, J. A. Programmed DNA Destruction by Miniature CRISPR-Cas14 Enzymes. *Science (80-.).* **2018**, *362* (6416), 839–842. https://doi.org/10.1126/science.aav4294.
(9) Kim, H.; Lee, S.; Seo, H. W.; Kang, B.; Moon, J.; Lee, K. G.; Yong, D.; Kang, H.; Jung, J.; Lim, E. K.; Jeong, J.; Park, H. G.; Ryu, C. M.; Kang, T. Clustered Regularly Interspaced Short Palindromic Repeats-Mediated Surface-Enhanced Raman Scattering Assay for Multidrug-Resistant Bacteria. *ACS Nano* **2020**, *14* (12), 17241–17253. https://doi.org/10.1021/acsnano.0c07264.
(10) Liang, M.; Li, Z.; Wang, W.; Liu, J.; Liu, L.; Zhu, G.; Karthik, L.; Wang, M.; Wang, K. F.; Wang, Z.; Yu, J.; Shuai, Y.; Yu, J.; Zhang, L.; Yang, Z.; Li, C.; Zhang, Q.; Shi, T.; Zhou, L.; Xie, F.; Dai, H.; Liu, X.; Zhang, J.; Liu, G.; Zhuo, Y.; Zhang, B.; Liu, C.; Li, S.; Xia, X.; Tong, Y.; Liu, Y.; Alterovitz, G.; Tan, G. Y.; Zhang, L. X. A CRISPR-Cas12a-Derived Biosensing Platform for the Highly Sensitive Detection of Diverse Small Molecules. *Nat. Commun.* **2019**, *10* (1), 1–9. https://doi.org/10.1038/s41467-019-11648-1.
(11) Dai, Y.; Somoza, R. A.; Wang, L.; Welter, J. F.; Li, Y.; Caplan, A. I.; Liu, C. C. Exploring the Trans-Cleavage Activity of CRISPR-Cas12a (Cpf1) for the Development of a Universal Electrochemical Biosensor. *Angewandte Chemie - International Edition*. 2019, pp 17399–17405. https://doi.org/10.1002/anie.201910772.
(12) Cheng, X.; Li, Y.; Kou, J.; Liao, D.; Zhang, W.; Yin, L.; Man, S.; Ma, L. Biosensors and Bioelectronics Novel Non-Nucleic Acid Targets Detection Strategies Based on CRISPR / Cas Toolboxes : A Review. *Biosens. Bioelectron.* **2022**, *215*, 114559. https://doi.org/10.1016/j.bios.2022.114559.
(13) Xiong, Y.; Zhang, J.; Yang, Z.; Mou, Q.; Ma, Y.; Xiong, Y.; Lu, Y. Functional DNA Regulated CRISPR-Cas12a Sensors for Point-of-Care Diagnostics of Non-Nucleic-Acid Targets. *J. Am. Chem. Soc.* **2020**, *142* (1), 207–213.

https://doi.org/10.1021/jacs.9b09211.
(14) Peng, L.; Zhou, J.; Liu, G.; Yin, L.; Ren, S.; Man, S.; Ma, L. CRISPR-Cas12a Based Aptasensor for Sensitive and Selective ATP Detection. *Sensors Actuators, B Chem.* **2020**, *320*, 128164. https://doi.org/10.1016/j.snb.2020.128164.
(15) Xu, Z.-H.; Zhao, Z.-Y.; Wang, H.; Wang, S.-M.; Chen, H.-Y.; Xu, J.-J. CRISPR-Cas12a-Based Efficient Electrochemiluminescence Biosensor for ATP Detection. *Anal. Chim. Acta* **2021**, *1188*, 339180. https://doi.org/https://doi.org/10.1016/j.aca.2021.339180.
(16) Niu, C.; Wang, C.; Li, F.; Zheng, X.; Xing, X.; Zhang, C. Aptamer Assisted CRISPR-Cas12a Strategy for Small Molecule Diagnostics. *Biosens. Bioelectron.* **2021**, *183*, 113196. https://doi.org/10.1016/j.bios.2021.113196.
(17) Li, C. Y.; Zheng, B.; Li, J. T.; Gao, J. L.; Liu, Y. H.; Pang, D. W.; Tang, H. W. Holographic Optical Tweezers and Boosting Upconversion Luminescent Resonance Energy Transfer Combined Clustered Regularly Interspaced Short Palindromic Repeats (Crispr)/Cas12a Biosensors. *ACS Nano* **2021**, *15* (5), 8142–8154. https://doi.org/10.1021/acsnano.0c09986.
(18) Wang, M.; Zuris, J. A.; Meng, F.; Rees, H.; Sun, S.; Deng, P.; Han, Y.; Gao, X.; Pouli, D.; Wu, Q. Efficient Delivery of Genome-Editing Proteins Using Bioreducible Lipid Nanoparticles. *Proc. Natl. Acad. Sci.* **2016**, *113* (11), 2868–2873. https://doi.org/10.1073/pnas.152024411.
(19) Yamagishi, A.; Matsumoto, D.; Kato, Y.; Honda, Y.; Morikawa, M.; Iwata, F.; Kobayashi, T.; Nakamura, C. Direct Delivery of Cas9-SgRNA Ribonucleoproteins into Cells Using a Nanoneedle Array. *Appl. Sci.* **2019**, *9* (5), 965. https://doi.org/10.3390/app9050965.
(20) Liu, J.; Wen, J.; Zhang, Z.; Liu, H.; Sun, Y. Voyage inside the Cell: Microsystems and Nanoengineering for Intracellular Measurement and Manipulation. *Microsystems Nanoeng.* **2015**, *1* (1), 15020. https://doi.org/10.1038/micronano.2015.20.
(21) Brooks, J.; Minnick, G.; Mukherjee, P.; Jaberi, A.; Chang, L.; Espinosa, H. D.; Yang, R. High Throughput and Highly Controllable Methods for In Vitro Intracellular Delivery. *Small* **2020**, *16* (51), 2004917. https://doi.org/10.1002/smll.202004917.
(22) Elnathan, R.; Barbato, M. G.; Guo, X.; Mariano, A.; Wang, Z.; Santoro, F.; Shi, P.; Voelcker, N. H.; Xie, X.; Young, J. L. Biointerface Design for Vertical Nanoprobes. *Nat. Rev. Mater.* **2022**, 1–21. https://doi.org/10.1038/s41578-022-00464-7.
(23) Chiappini, C. Nanoneedle-Based Sensing in Biological Systems. *ACS sensors* **2017**, *2* (8), 1086–1102. https://doi.org/10.1021/acssensors.7b00350.
(24) Chiappini, C.; De Rosa, E.; Martinez, J. O.; Liu, X.; Steele, J.; Stevens, M. M.; Tasciotti, E. Biodegradable Silicon Nanoneedles Delivering Nucleic Acids Intracellularly Induce Localized in Vivo Neovascularization. *Nat. Mater.* **2015**, *14* (5), 532–539. https://doi.org/10.1038/nmat4249.
(25) Gopal, S.; Chiappini, C.; Penders, J.; Leonardo, V.; Seong, H.; Rothery, S.; Korchev, Y.; Shevchuk, A.; Stevens, M. M. Porous Silicon Nanoneedles Modulate Endocytosis to Deliver Biological Payloads. *Adv. Mater.* **2019**, *31* (12), 1806788. https://doi.org/10.1002/adma.201806788.
(26) Hansel, C. S.; Crowder, S. W.; Cooper, S.; Gopal, S.; João Pardelha da Cruz, M.; de Oliveira Martins, L.; Keller, D.; Rothery, S.; Becce, M.; Cass, A. E. G. Nanoneedle-Mediated Stimulation of Cell Mechanotransduction Machinery. *ACS Nano* **2019**, *13* (3), 2913–2926. https://doi.org/10.1021/acsnano.8b06998.
(27) Chiappini, C.; Martinez, J. O.; De Rosa, E.; Almeida, C. S.; Tasciotti, E.; Stevens, M. M. Biodegradable Nanoneedles for Localized Delivery of Nanoparticles in Vivo:

Exploring the Biointerface. *ACS Nano* **2015**, *9* (5), 5500–5509. https://doi.org/10.1021/acsnano.5b01490.
(28) Chiappini, C.; Chen, Y.; Aslanoglou, S.; Mariano, A.; Mollo, V.; Mu, H.; De Rosa, E.; He, G.; Tasciotti, E.; Xie, X. Tutorial: Using Nanoneedles for Intracellular Delivery. *Nat. Protoc.* **2021**, *16* (10), 4539–4563. https://doi.org/10.1038/s41596-021-00600-7.
(29) Kooger, R.; Zambelli, T.; Julia, A.; Guillaume-gentil, O.; Grindberg, R. V; Kooger, R.; Dorwling-carter, L.; Martinez, V. Tunable Single-Cell Extraction for Molecular Resource Tunable Single-Cell Extraction for Molecular Analyses. *Cell* **2016**, *166* (2), 506–516. https://doi.org/10.1016/j.cell.2016.06.025.
(30) Cao, Y.; Hjort, M.; Chen, H.; Birey, F.; Leal-Ortiz, S. A.; Han, C. M.; Santiago, J. G.; Paşca, S. P.; Wu, J. C.; Melosh, N. A. Nondestructive Nanostraw Intracellular Sampling for Longitudinal Cell Monitoring. *Proc. Natl. Acad. Sci.* **2017**, *114* (10), E1866–E1874. https://doi.org/10.1073/pnas.1615375114.
(31) Wang, Z.; Qi, L.; Yang, Y.; Lu, M.; Xie, K.; Zhao, X.; Cheung, E. H. C.; Wang, Y.; Jiang, X.; Zhang, W. High-Throughput Intracellular Biopsy of MicroRNAs for Dissecting the Temporal Dynamics of Cellular Heterogeneity. *Sci. Adv.* **2020**, *6* (24), eaba4971. https://doi.org/10.1126/sciadv.aba4971.
(32) Xie, K.; Wang, Z.; Qi, L.; Zhao, X.; Wang, Y.; Qu, J.; Xu, P.; Huang, L.; Zhang, W.; Yang, Y. Profiling MicroRNAs with Associated Spatial Dynamics in Acute Tissue Slices. *ACS Nano* **2021**, *15* (3), 4881–4892. https://doi.org/10.1021/acsnano.0c09676.
(33) Chen, W.; Guillaume-Gentil, O.; Rainer, P. Y.; Gäbelein, C. G.; Saelens, W.; Gardeux, V.; Klaeger, A.; Dainese, R.; Zachara, M.; Zambelli, T. Live-Seq Enables Temporal Transcriptomic Recording of Single Cells. *Nature* **2022**, 1–8. https://doi.org/10.1038/s41586-022-05046-9.
(34) Hardie, D. G.; Ross, F. A.; Hawley, S. A. AMPK: A Nutrient and Energy Sensor That Maintains Energy Homeostasis. *Nat. Rev. Mol. cell Biol.* **2012**, *13* (4), 251–262. https://doi.org/10.1038/nrm3311.
(35) Biswas, S.; Kinbara, K.; Niwa, T.; Taguchi, H.; Ishii, N.; Watanabe, S.; Miyata, K.; Kataoka, K.; Aida, T. Biomolecular Robotics for Chemomechanically Driven Guest Delivery Fuelled by Intracellular ATP. *Nat. Chem.* **2013**, *5* (7), 613–620. https://doi.org/10.1038/nchem.1681.
(36) Hong, S.; Pedersen, P. L. ATP Synthase and the Actions of Inhibitors Utilized to Study Its Roles in Human Health, Disease, and Other Scientific Areas. *Microbiol. Mol. Biol. Rev.* **2008**, *72* (4), 590–641. https://doi.org/10.1128/MMBR.00016-08.
(37) Li, A.; Gao, M.; Liu, B.; Qin, Y.; chen, L.; Liu, H.; Wu, H.; Gong, G. Mitochondrial Autophagy: Molecular Mechanisms and Implications for Cardiovascular Disease. *Cell Death Dis.* **2022**, *13* (5), 1–15. https://doi.org/10.1038/s41419-022-04906-6.
(38) de Vries, D. D.; van Engelen, B. G. M.; Gabreëls, F. J. M.; Ruitenbeek, W.; van Oost, B. A. A Second Missense Mutation in the Mitochondrial ATPase 6 Gene in Leigh's Syndrome. *Ann. Neurol. Off. J. Am. Neurol. Assoc. Child Neurol. Soc.* **1993**, *34* (3), 410–412.
(39) Murphy, M. P.; Hartley, R. C. Mitochondria as a Therapeutic Target for Common Pathologies. *Nat. Rev. Drug Discov.* **2018**, *17* (12), 865–886. https://doi.org/10.1038/nrd.2018.174.
(40) Davalos, D.; Grutzendler, J.; Yang, G.; Kim, J. V; Zuo, Y.; Jung, S.; Littman, D. R.; Dustin, M. L.; Gan, W.-B. ATP Mediates Rapid Microglial Response to Local Brain Injury in Vivo. *Nat. Neurosci.* **2005**, *8* (6), 752–758. https://doi.org/10.1038/nn1472.
(41) Khakh, B. S.; Alan North, R. P2X Receptors as Cell-Surface ATP Sensors in Health and Disease. *Nature* **2006**, *442* (7102), 527–532. https://doi.org/10.1038/nature04886.

(42) Lin, M. T.; Beal, M. F. Mitochondrial Dysfunction and Oxidative Stress in Neurodegenerative Diseases. *Nature* **2006**, *443* (7113), 787–795. https://doi.org/10.1038/nrd.2018.174.
(43) Wallace, D. C. Mitochondrial Diseases in Man and Mouse. *Science (80-.).* **1999**, *283* (5407), 1482–1488. https://doi.org/10.1038/s41419-022-04906-6.
(44) Hannah, R.; Beck, M.; Moravec, R.; Riss, T. CellTiter-Glo™ Luminescent Cell Viability Assay: A Sensitive and Rapid Method for Determining Cell Viability. *Promega Cell Notes* **2001**, *2*, 11–13.
(45) Gordon, M. J.; Huang, X.; Pentoney Jr, S. L.; Zare, R. N. Capillary Electrophoresis. *Science (80-.).* **1988**, *242* (4876), 224–228. https://doi.org/10.1126/science.242.4876.224.
(46) Jang, C.; Chen, L.; Rabinowitz, J. D. Metabolomics and Isotope Tracing. *Cell* **2018**, *173* (4), 822–837. https://doi.org/10.1016/j.cell.2018.03.055.
(47) Hahn-Windgassen, A.; Nogueira, V.; Chen, C.-C.; Skeen, J. E.; Sonenberg, N.; Hay, N. Akt Activates the Mammalian Target of Rapamycin by Regulating Cellular ATP Level and AMPK Activity. *J. Biol. Chem.* **2005**, *280* (37), 32081–32089. https://doi.org/10.1074/jbc.M502876200.
(48) Imamura, H.; Huynh Nhat, K. P.; Togawa, H.; Saito, K.; Iino, R.; Kato-Yamada, Y.; Nagai, T.; Noji, H. Visualization of ATP Levels inside Single Living Cells with Fluorescence Resonance Energy Transfer-Based Genetically Encoded Indicators. *Proc. Natl. Acad. Sci.* **2009**, *106* (37), 15651–15656. https://doi.org/10.1073/pnas.0904764106.
(49) Wang, Y.; Yang, Y.; Yan, L.; Kwok, S. Y.; Li, W.; Wang, Z.; Zhu, X.; Zhu, G.; Zhang, W.; Chen, X. Poking Cells for Efficient Vector-Free Intracellular Delivery. *Nat. Commun.* **2014**, *5* (1), 1–9.
(50) Beis, I.; Newsholme, E. A. The Contents of Adenine Nucleotides, Phosphagens and Some Glycolytic Intermediates in Resting Muscles from Vertebrates and Invertebrates. *Biochem. J.* **1975**, *152* (1), 23–32. https://doi.org/10.1042/bj1520023.